Chapter 5

Crystal growth in a three-phase system: Diffusion and liquid-liquid phase separation in lysozyme crystal growth

In the phase diagram of the protein hen egg-white lysozyme, a region is present in which the lysozyme solution demixes and forms two liquid phases. In-situ observations by optical microscopy show the dense liquid droplets to dissolve when crystals grow in this system. During this process the demixed liquid region retracts from the crystal surface. The spatial distribution of the dense phase droplets present a special kind of boundary conditions for Fick's second law for diffusion. In combination with the cylindrical symmetry provided by the kinetically roughened crystals, this system allows for a full numerical analysis. Using experimental data for setting the boundary conditions, a quasi-steady-state solution for the time-dependent concentration profile was shown to be valid. Comparison of kinetically rough growth in a phase separated system and in a non-separated system shows the growth kinetics for a three-

phase system to differ from a two-phase system, in that crystals grow more slowly but the duration of growth is prolonged.

5.1 Introduction

The capability of concentrated lysozyme solutions to undergo a separation into two liquid phases was first indicated by light scattering from unbuffered lysozyme-salt solutions[1]. Later, observations of liquid-liquid phase separation in buffered lysozyme solutions[2] and also other protein solutions followed [3, 4]. A phase diagram for the lysozyme-chloride system, indicating the binodal and spinodal of the metastable liquid-liquid separation, has been well established[5, 6]. L-L phase separation is relevant for protein crystallization, because cycling through the binodal into the two-phase region and back promotes nucleation of crystals[5], as does choosing crystallization conditions near the L-L coexistence line[7].

Although the mechanism of forming a low and high protein concentration phase would suggest crystal nucleation to occur in the dense liquid phase, for lysozyme it was found that due to gel formation, kinetics in these high-density droplets are arrested[5, 8] and thus nucleation is inhibited. Optical micrographs showing the growth of crystals in the presence of droplets of the dense liquid phase provide evidence that the dense liquid droplets do not cause the nucleation of new crystals[8, 9]. The disappearance of the dense phase around the crystal phase indicates a depletion zone due to the growing crystal[10–12]. The depletion of the dilute phase results in the dense phase dissolving into the dilute phase to locally restore the equilibrium concentration of this phase in contact with the dense phase.

In this paper, we specifically investigate the dissolution of the dense phase and its spatial distribution with respect to growing crystals. Previously, L-L phase separation was used to maintain a constant surface concentration during spherulitic growth of lysozyme[13]. Here, on the contrary, we use the retracting dense phase as an iso-concentration line in a diffusive system. The system presents a diffusion problem with two moving boundaries, and a special

condition due to the dense liquid phase dissolving into the dilute phase. A numerical analysis is presented showing the kinetics to be different from the case of diffusion without L-L phase separation. This represents a general case of crystal growth in a three-phase system in which a solid or liquid metastable phase dissolves, while a stable phase grows.

5.2 Experimental methods

Hen egg-white lysozyme from Sigma-Aldrich (lot nr. 094K1454) and chemicals of analytical grade were used in this study. A buffer stock solution of sodium acetate and acetic acid was made in deionized water (>15 MΩcm) to result in a 0.05 M $NaCH_3COO/HCH_3COO$ solution of pH 4.5. A stock lysozyme solution was prepared by dissolving the lysozyme in the buffer solution and filtering this solution over a 0.2 μm membrane (Schleicher & Schuell). A sodium-chloride stock solution was also prepared in buffer solution and filtered. Lysozyme, NaCl and buffer solutions were mixed with each other in the appropriate proportions just prior to the growth experiments. All experiments performed used a sodium chloride concentration of 0.685 M (i.e. 4% w/v), because for this concentration literature provides phase diagrams on the liquid-liquid coexistence line[6, 8].

After mixing, a droplet of 10 μl is placed on a sapphire substrate and covered by a thin glass slide, forming an approximately 100 μm thick liquid layer, and is sealed off at the sides by vacuum grease to prevent evaporation. Performing the experiment in a thin layer prevents convection to occur and allows for better optical images of both the crystals and the spatial distribution of the dense droplets in the plane of projection. Next, the sample is placed on a precooled, temperature-controlled stage and covered by a brass plate to bring the solution into the demixing region of the phase diagram by cooling down. A 6 mm hole in the temperature-controlled stage and a 15 mm hole in the brass cover plate allow for transmission optical microscopy. The temperatures of the stage and cover plate were monitored by thermocouples and found to differ at most 0.3 ^oC.

Observations were made by transmission optical microscopy using a Nikon Microphot-88. The optical micrographs were recorded using a microscope mounted CCD camera (Nikon DS5M). Data on growth kinetics and droplet dissolution rates were determined from subsequent images with the aid of image processing software (Image-Pro Plus).

5.3 Results and Discussion

5.3.1 Liquid-liquid phase separation and kinetic roughening

In figure 5.1 we present a series of optical micrographs of a growing tetragonal lysozyme crystal surrounded by a phase-separated solution. After cooling down the solution containing 37.4 mg/ml HEWL to 8.1 ^oC, dense liquid phase droplets formed. The sample was checked for crystals to nucleate, and once found these crystals were observed during growth. The crystals start out kinetically rough, and appear circular in the images. Patterns on the surface indicate the four-fold axis of the $P4_32_12$ structure of tetragonal lysozyme to point out of the plane of projection (i.e. the {101} faces grow tilted with respect to the image plane, while the {110} faces are oriented perpendicular to the image plane). Around the crystal an area develops in which no high-density droplets are present. The outer border of this area moves away from the crystal surface as time progresses, while the crystal continues to grow. In the end all dense liquid droplets have dissolved and the crystal has become square.

Figure 5.2a shows a schematic phase diagram of the lysozyme-NaCl-buffer system. The liquidus and solidus indicate the equilibrium concentration of protein in the liquid and crystalline phase respectively, at given temperature. Mixtures in between these two lines will eventually separate in a solid, crystalline phase and a saturated solution. In this phase region, a metastable liquid-liquid miscibility dome is present. Mixtures in this region will separate in two liquid phases, of which the lower density phase subsequently separates into solid and liquid (fig. 5.2b). The concentration of the dilute phase drops as a result of the formation of the solid phase. As the dilute phase leaves the

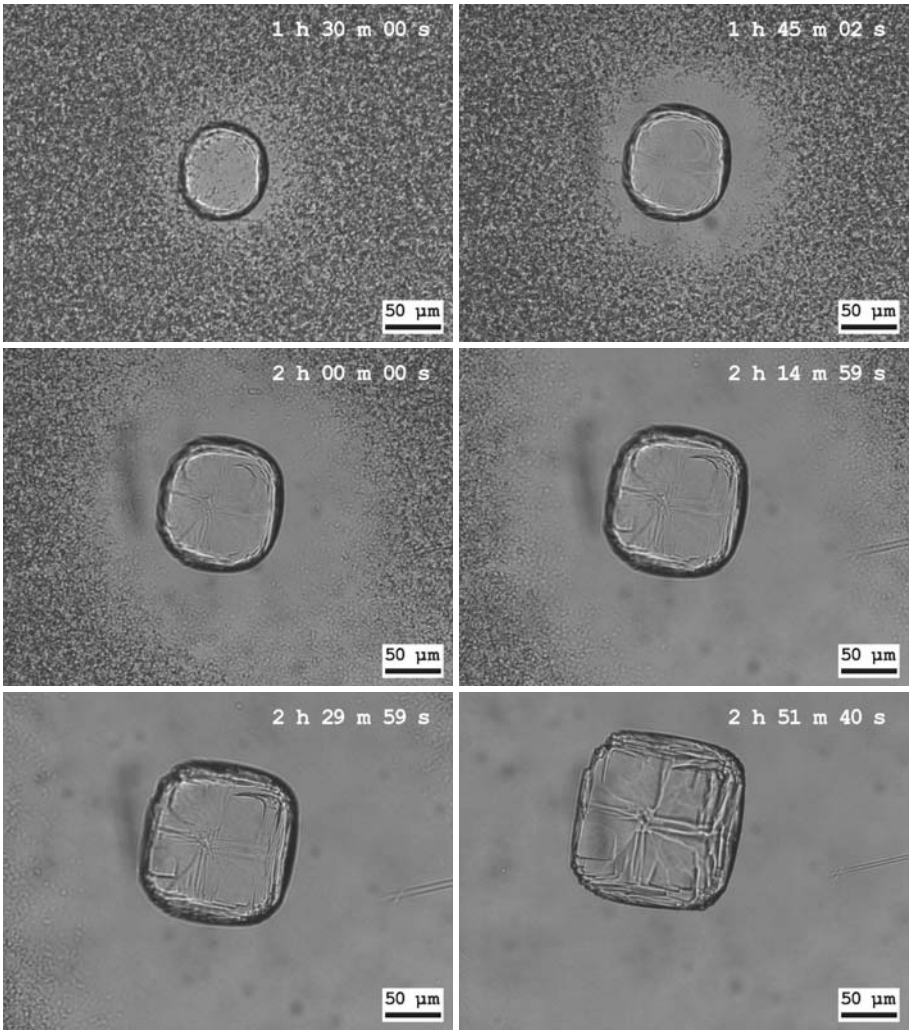

Figure 5.1: Optical micrographs of a tetragonal lysozyme crystal surrounded by a L-L phase separated solution at 8.1 ^{o}C. The crystal starts out kinetically rough, but as the surface concentration drops it becomes faceted. The high-density droplets dissolve into the low-density solution as a result of the low-density solution being depleted by the growing crystal. Before phase separation, the mother liquor consisted of 37.4 mg/ml HEWL, 0.685 M NaCl in a 0.05 M NaOAc/HOAc buffered solution at pH 4.5. The time in the upper right corner of the images indicates the time since cooling down below T_{cloud}.

liquid-liquid coexistence line, the dense phase dissolves into the dilute phase in an attempt to retain equilibrium (dotted arrow in fig. 5.2). The spatial distribution of the two-liquid-phases region is a result of the nucleation and growth of crystals in the dilute liquid. Figure 5.2c shows a micrograph of several crystals growing in a L-L phase separated region. Around the crystals depleted zones are visible, roughly following the shapes and positions of the crystals. Here, the high density droplets have dissolved, from which we conclude that the local concentration is lower than the dilute phase of the liquid-liquid coexistence (left dot in fig. 5.2b). At the edge of the depletion zone, the solution is in equilibrium with the dense solution droplets. Thus, this edge functions as an iso-concentration line and has the concentration of the low-density liquid.

At the beginning of the experiment, crystals nucleate in the low-concentration part of the solution. These crystals start out as circular crystals, but turn square in the course of the experiment (fig. 5.1). The rounded shape of the crystals indicates kinetic roughening of the surface[11, 14]. The mechanism by which a crystal grows depends on the supersaturation, σ. When the supersaturation is increased around a certain crossover supersaturation, σ_{tr}, the mechanism gradually changes from 2D nucleation to growth by continuous addition[11]. This transition to the kinetic roughening regime is a result of the supersaturation becoming so high that the critical nucleus for 2D nucleation, given by

$$r_{\mathrm{c}} = \frac{\Omega\gamma}{\Delta\mu\, h_{\mathrm{st}}} \ , \tag{5.1}$$

becomes equal to or smaller than the radius of one growth unit. In this equation γ is the edge free energy, and $\Delta\mu$ is the difference in chemical potential between liquid and solid phase. Further, Ω is the volume of a growth unit and h_{st} is the height of a growth layer. The thermodynamic supersaturation is linked to the chemical potential difference via $\frac{\Delta\mu}{kT} = \ln\frac{c}{c_{\mathrm{eq}}} \equiv \sigma$ (for an ideal solution). Thus, the change from a rounded shape into a square shape indicates a drop in concentration at the crystal surface during growth, in compliance with the dissolution of the dense liquid droplets near the crystal.

During a number of our experiments spherulites were formed simultane-

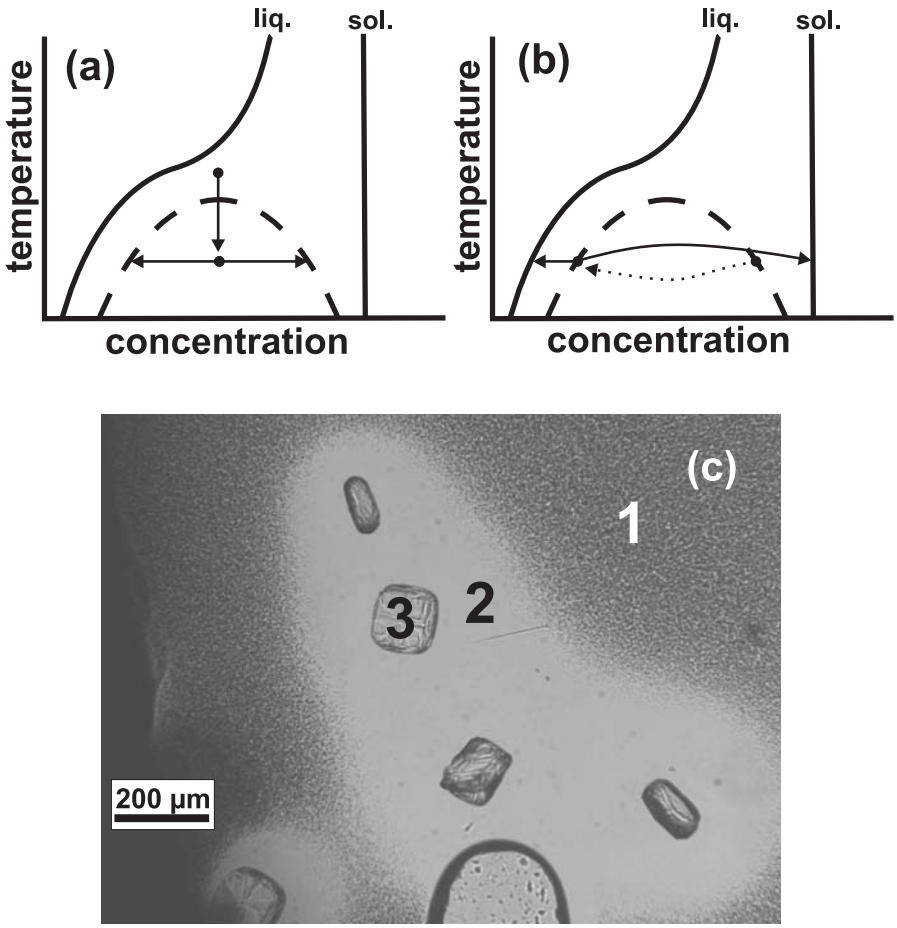

Figure 5.2: (a) Schematic phase diagram of the lysozyme-NaCl-buffer system. Experiments start out in the mixed phase between solidus and liquidus, and are brought into the liquid-liquid demixing region by cooling down (vertical arrow). The solution demixes and forms dense droplets in a diluted solution (horizontal arrows). The dense droplets gelate and kinetics are arrested. (b) The dilute solution, still between solidus and liquidus, separates in a solid, crystalline phase and an even more diluted solution (solid arrows). To maintain equilibrium with the dilute phase, the dense droplets dissolve into the dilute phase (dotted arrow). (c) Optical micrograph showing three phases of the lysozyme system simultaneously. The dense droplets (1) dissolve into the dilute phase as the growing crystals (3) deplete their surroundings (2).

ously with the tetragonal crystals. In reference [12] we showed that regular crystal or spherulite growth is not necessarily related to the occurrence of the liquid-liquid phase separation. In this paper the spherulites are not further considered.

5.3.2 Droplet distribution and diffusion

From the optical images of the series in figure 5.1, the crystal growth rate and the dense droplet retraction rate are determined. Figure 5.3a shows the crystal size as function of time for two <110> directions and one <100> direction. At 2.5 hours after cooling down, the crystal starts to become faceted, i.e. the <100> direction grows faster than <110>. The change from kinetic roughening to 2D nucleation growth is a gradual transition. After an initial period (t <1.5 hrs), the dense droplets dissolve and "retract" from the crystal surface faster than the crystal grows (fig. 5.3b). The L-L phase separation boundary retracts from the crystal surface at 210 μm/hour, while the crystal grows at a rate of 57 μm/hour.

Using the kinetics of crystal growth rate and dense droplet dissolution rate, the concentration profile in the system can be evaluated. Due to the thin geometry of the system, convection can be neglected. Mass transport in the system follows Fick's laws of diffusion. Fick's second law gives a time-dependent concentration field, by

$$\frac{\partial c(\vec{r},t)}{\partial t} = D\nabla^2 c(\vec{r},t) \ , \tag{5.2}$$

with $c(\vec{r},t)$ the lysozyme concentration at position $\vec{r}$ at time t, and D the diffusion coefficient. The combination of kinetically rough and approximately circular crystals, and the circular pattern of dissolving dense droplets allows the use of radial symmetry in solving equation 5.2 (see fig. 5.4). For the {101} faces the roughening transition is at higher supersaturations, and in the experiments these faces grow much slower than the {110} faces and thus have far less influence on the concentration profile. Regarding the growing crystal as a cylinder (fig. 5.4), the diffusion equation can be written in the cylindrical

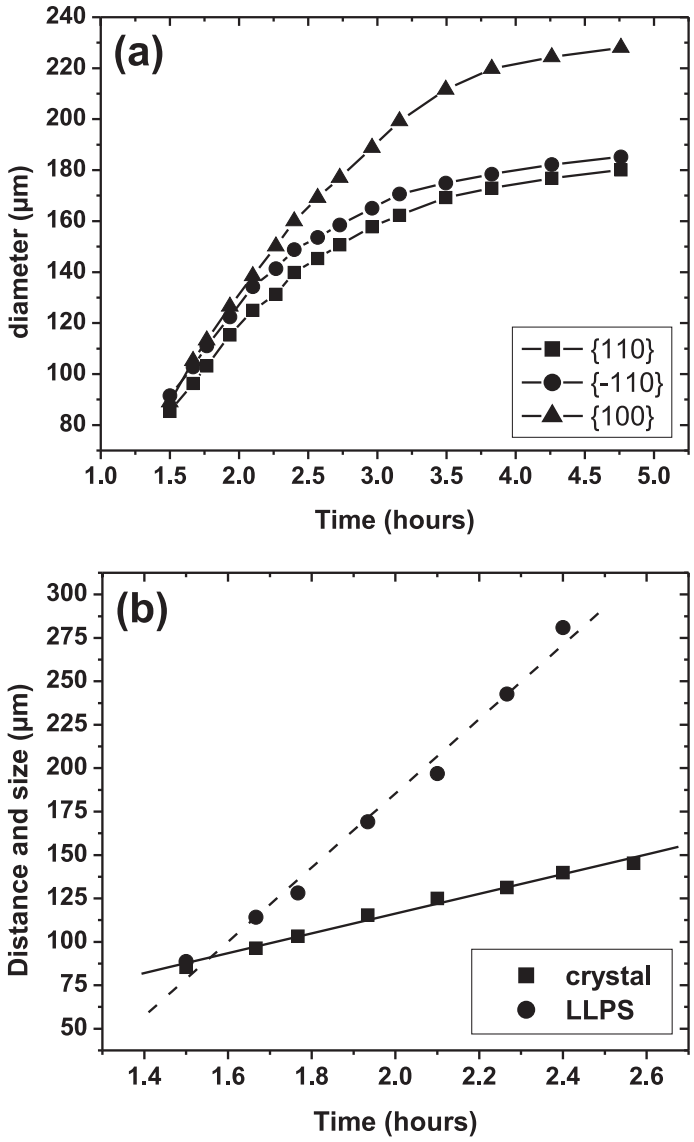

Figure 5.3: Data taken from the optical micrographs of figure 5.1. (a) Crystal size as function of time. (b) Size of the crystal and distance of the L-L phase separation boundary. The crystal grows at 57 μm/hour (slope of solid line), and the phase separation boundary retracts away from the crystal surface with 210 μm per hour (slope of dashed line).

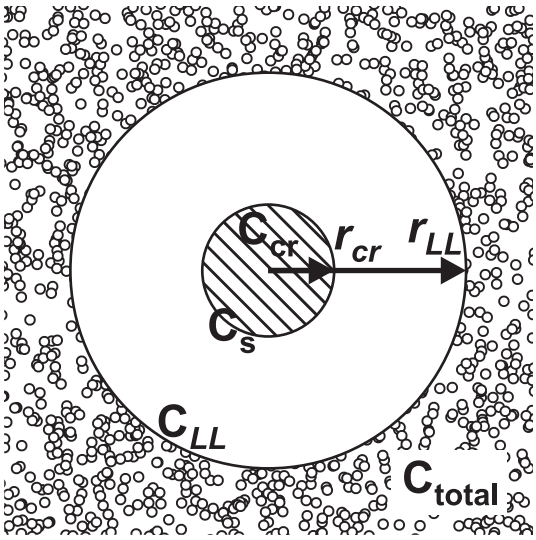

Figure 5.4: Schematic representation of a kinetically rough crystal growing from a L-L phase separated solution.

symmetric form:

$$\frac{\partial c(r,t)}{\partial t} = D\frac{\partial^2 c(r,t)}{\partial r^2} + \frac{D}{r}\frac{\partial c(r,t)}{\partial r} \ . \tag{5.3}$$

The solution of this equation depends on the boundary conditions. Experiments provide us with a set of boundary conditions, as the position of the crystal surface and the position of the L-L phase separation boundary at a certain time can be taken from the experimental data of figure 5.3. The concentration profile in between these boundaries follows from solving equation 5.3. The boundary condition at the crystal surface is determined by the flux at the surface. The flux across the crystal surface is determined by the crystal growth rate on the one hand, and by the concentration gradient at the surface on the other hand. The growth rate for kinetically roughened faces is given by[14, 15]

$$v_{\mathrm{crys}} = \beta(c_{\mathrm{s}} - c_{\mathrm{tr}}) \ , \tag{5.4}$$

with β a kinetic coefficient* in $m^4\, s^{-1}\, g^{-1}$, c_{s} the surface concentration, and c_{tr}

*We assume the crystal to fill completely the vertical space in the growth cell. Finite

the cross-over concentration for kinetically roughened growth. For lysozyme, the cross-over concentration is 7.7 times the equilibrium concentration of the liquid phase[15], i.e. $c_{\mathrm{tr}} = 7.7 c_{\mathrm{eq}}$. The mass flux into the crystal surface due to growth is given by

$$J_{\mathrm{cr}} = v_{\mathrm{crys}} \cdot c_{\mathrm{cr}} = \beta \; c_{\mathrm{cr}}(c_{\mathrm{s}} - c_{\mathrm{tr}}) \; , \tag{5.5}$$

in which c_{cr} is the lysozyme concentration in the tetragonal crystalline lysozyme phase. The diffusional mass flux at the crystal surface is given by

$$J_D = -D \frac{\partial c}{\partial r} \; . \tag{5.6}$$

The diffusional flux J_D is equal to the growth flux J_{cr}, and both give an expression for the relation between surface concentration and concentration gradient:

$$\frac{\partial c}{\partial r} = \frac{\beta c_{\mathrm{cr}}}{D}(c_{\mathrm{s}} - c_{\mathrm{tr}}) \; . \tag{5.7}$$

The edge of the L-L phase separation region provides the outer boundary conditions for the radial diffusion equation. Here, at $r = r_{\mathrm{LL}}$, the concentration is equal to the dilute phase concentration, c_{LL} (see figure 5.4), because dilute and dense phase are exactly in equilibrium. If for each moment in time the system is considered to be in a steady state, the time-independent diffusion equation can be used. In combination with the boundary conditions this leads to the solution[16]:

$$c(r) = \frac{c_{\mathrm{tr}} r_{\mathrm{cr}} h \ln(r_{\mathrm{LL}}/r) + c_{\mathrm{LL}}(1 + r_{\mathrm{cr}} h \ln(r/r_{\mathrm{cr}})}{1 + r_{\mathrm{cr}} h \ln(r_{\mathrm{LL}}/r_{\mathrm{cr}})} \; , \tag{5.8}$$

with r_{cr} the radius of the crystal, and h is $\beta c_{\mathrm{cr}}/D$. The radii r_{cr} and r_{LL} are taken from experiment, and the physical parameters are taken from literature (see table 5.1). Figure 5.5 shows the concentration profiles at the various instances in time using this quasi-steady-state solution.

---

elements calculations show that the concentration profile qualitatively remains the same when the crystal does not completely fills the vertical space. The effect on the boundary conditions is that we have an effective $\beta' = \beta \cdot h_{\mathrm{crystal}}/h_{\mathrm{cell}}$.

To evaluate if the quasi-steady-state approximation holds, we use the position of the crystal surface and phase separation as boundaries in a numerical solution of Fick's time-dependent equation by the finite differences method [16]. In this method, both time and radius are divided into discrete sections, and equation 5.3 can be written in a discrete form

$$\frac{c_i^{j+1} - c_i^j}{\Delta t} = \frac{D}{2i(\Delta r)^2}\left[(2i+1)c_{i+1}^j - 4ic_i^j + (2i-1)c_{i-1}^j\right] , \qquad (5.9)$$

in which c_i^j is the the concentration of the i^{th} section of width Δr during the j^{th} time section of length Δt. From equation 5.9 an expression for the concentration of the i^{th} section at time j+1, c_i^{j+1} can be derived. We have calculated the time-dependent concentration profile using Matlab[17]. The positions of the moving boundaries, i.e. $r_{\text{cr}}(t)$ and $r_{\text{LL}}(t)$, are taken from experiment. Equation 5.7 and $c(r_{\text{LL}}) = c_{\text{LL}}$ are used at these boundaries similar to the quasi-steady-state case. The resulting concentration profiles (dashed lines in figure 5.5) show good agreement with the quasi-steady-state approximation. Thus, the quasi-steady-state model is a valid approximation. The surface concentration remains much higher than the equilibrium concentration (at least a factor 20), indicating that although the crystal grows kinetically rough, surface kinetics still play a major role in the growth process. This property of lysozyme crystal growth differs fundamentally from the kinetically rough growth of small molecules, in which rough growth depletes the surrounding solution to its equilibrium concentration and eventually leads to morphological instabilities. Here, the crystals grow rough, but do not loose their rounded shape. Although for a rough lysozyme crystal the critical nucleus has the size of one growth unit, the attachment of a properly oriented growth units takes more effort than for small molecules, and a barrier for incorporation still exists.

5.3.3 Two-phase system versus three-phase system

To investigate the difference between crystals growing in a L-L phase separated solution and those growing from a normal lysozyme solution, an experiment

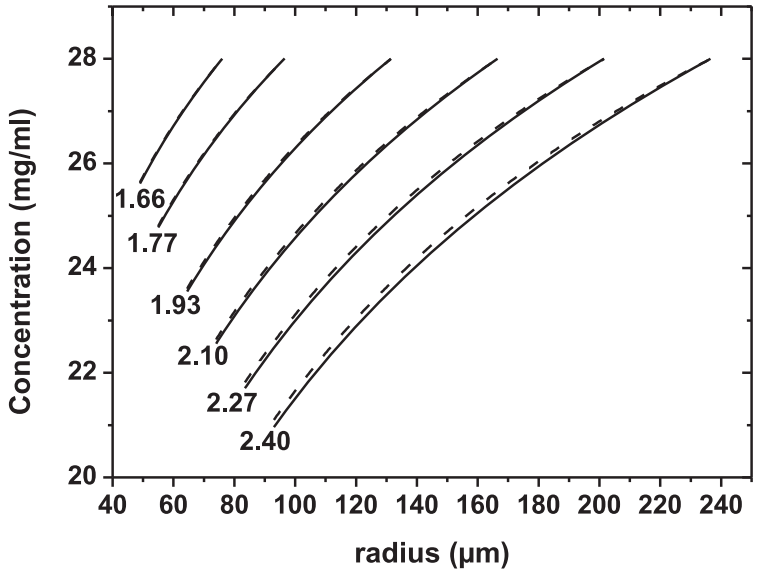

Figure 5.5: Concentration profiles at successive moments calculated using a quasi-steady-state approximation. The numbers indicate time in hours. The dashed lines indicate the time-dependent solution at the same instance calculated using finite differences. Data are taken from the experiment of figure 5.1

Table 5.1: Physical parameters taken from literature for finite differences calculations on the time-dependent diffusion equation, and for the quasi-steady-state calculations. c_{cr} is derived from the cell parameters of tetragonal lysozyme crystals and the molecular weight of lysozyme.

Parameter	Value	Ref.
β	$5{\times}10^{-8}\ cm^4\, s^{-1}\, mg^{-1}$	[15]
D	$8{\times}10^{-7}\ cm^2\, s^{-1}$	[18]
c_{equi}	$0.99\ mg/ml$	[19]
c_{tr}	$7.6\ mg/ml$	[15]
c_{LL}	$28\ mg/ml$	[6]
c_{cr}	$810\ mg/ml$	

was performed slightly above the L-L coexistence line at 8.5 ^{o}C. Here crystals also grow kinetically rough, but no dense liquid droplets are present in the vicinity. As the temperature difference between both experiments is minimal, we can consider the various constants, β, D, c_{equi} and c_{tr}, as identical, which allows for comparison between a system with and without L-L phase separation. Figure 5.6a shows the crystal size versus time for this experiment as well as that of the experiment at 8.1 ^{o}C, which includes phase separation. The crystal growing from the normal solid-liquid phase has a higher growth rate, but the growth rate drops more abrupt. With respect to the demixed system, the mixed system implies a higher supersaturation, as the lysozyme concentration here is higher than in the dilute phase of the L-L coexistence region. Temperature also influences the supersaturation, but works in favour of the demixed experiment and cannot be responsible for the difference in growth kinetics. Due to the absence of the dense liquid droplets, we cannot use these as an outer boundary condition in the quasi-steady-state approximation. Using a finite differences method, the time-dependent diffusion equations can be solved to investigate the differences in growth kinetics, now using different boundary conditions for the two experiments. Instead of using growth data to determine the boundary conditions, the fluxes at the interfaces are used to determine their movement. The growth rate of the crystal surface, $\frac{\mathrm{d}r_{\mathrm{cr}}}{\mathrm{d}t}$, follows from equation 5.4, and is the driving force for the formation of a concentration gradient at the surface. The flux at the crystal-solution interface is given by eqs. 5.6 and 5.7. For the flux at the boundary of the L-L phase separated region we can write

$$J = (c_{\mathrm{total}} - c_{\mathrm{LL}})\frac{\mathrm{d}r_{\mathrm{LL}}}{\mathrm{d}t} \ , \tag{5.10}$$

with c_{total} the effective concentration of dilute and dense phase combined. In the same manner as for the flux at the crystal surface, this flux is equal to the diffusional flux at the phase separation interface, resulting in

$$\frac{\mathrm{d}r_{\mathrm{LL}}}{\mathrm{d}t} = \frac{D}{c_{\mathrm{total}} - c_{\mathrm{LL}}}\frac{\partial c}{\partial r}\bigg|_{r_{\mathrm{LL}}} \ . \tag{5.11}$$

In contrast to the situation at the crystal surface, here we do not have an expression for the speed of the phase boundary. As the droplet surfaces are

rough and disordered and the surface-volume ratio is large, they can be considered to have an infinitely large kinetic coefficient for dissolution. Therefore, besides the flux boundary condition, a second boundary condition is given by the constant concentration as a result of the dissolution at an "infinitely" high rate, $c(r_{\mathrm{LL}}) = c_{\mathrm{LL}}$. The displacement of the L-L phase separation boundary now follows from the constant concentration at the boundary and the expression for the flux. For the system without phase separation present, at the outer boundary (the size of the growth cell or half the average distance between neighboring crystals), the concentration can change freely, but no flux of mass into the system is present, thus mimicking a finite system. The same boundary condition is used for the system *with* demixing at the moment the phase separation reaches the edge of the system. Figure 5.6b shows the calculated size of the crystal in both systems as function of time. Quantitatively, the calculated sizes do not fit the experiment completely, but qualitatively they do show the same sharp decrease of growth rate at 2.5-3 hours as the experimental data. Presumably this difference can be accounted for that depending on the quality of the lysozyme the actual values of the parameters given in table 5.1 might be slightly different. An important factor influencing the calculations is the choice of the size of the system. In an experiment, crystals in each others vicinity influence each others diffusion field and thus determine the "effective" system size. The moment of the sharp decrease in the crystal growth rate depends on the distance between adjacent crystals or the edge of the system. The calculations indeed show the unmixed system to grow faster than the demixed system, and also indicates a more abrupt stop in growth rate. Thus, the presence of the phase separation adds an extra step in the process of the material supply to the crystal surface by its dissolution, which leads to a different growth behaviour. The experiments show that the surroundings of a crystal influences growth kinetics and should be taken into account when interpreting the results of a crystallization experiment. These findings also hold for crystal growth systems with less constraining geometry, as long as convection is supressed so that the 3D versions of Fick's laws can be used. Such systems are crystal growth in microgravity[20], gels[21], nanoliter

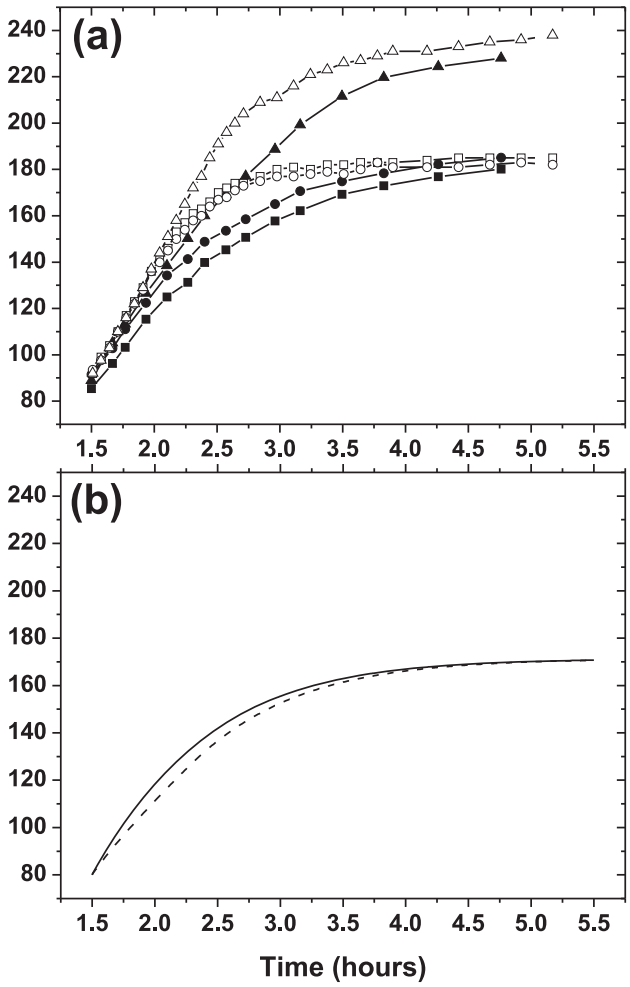

Figure 5.6: (a) Crystal size versus time for a kinetically rough crystal growing from a L-L phase separated system (solid symbols), and for a rough crystal growing in a system without L-L phase separation (open symbols). The squares and circles indicate the (110) and $(1\bar{1}0)$ direction respectively, and the triangles indicate the (100) direction. (b) Crystal size for a system without (solid line) and with (dashed line) L-L phase separation modeled by using the finite differences method and boundary conditions as specified in the text. The physical parameters used are given in table 5.1; the effective radius of the finite growth system is 400 μm.

volumes[22], and strong inhomogeneous magnetic fields[23].

5.4 Conclusion

Hen egg-white lysozyme crystals growing in a liquid-liquid phase separated solution deplete their surroundings from growth units. The spatial distribution of the dissolving dense liquid droplets directly visualizes the role of mass transport in a diffusive lysozyme crystal growth system. The edge of the depleted zone can be seen as an iso-concentration line and therefore can be used as a boundary condition in calculations on diffusion. Crystals rounded as a consequence of kinetically rough growth allow for cylindrical symmetry to be applied in solving the diffusion equations. Finite differences calculations show that a quasi-steady-state approximation can be used to describe the time-dependent diffusion field using boundary displacements from experiment. Comparison of systems with and without liquid-liquid phase separation show that the presence of the phase separation alters the boundary conditions and thus the growth kinetics. To conclude, the lysozyme-NaCl system offers an interesting means of investigating mass transport in crystal growth, influenced by the presence of an extra metastable liquid or solid phase.

The authors like to thank dr. H. Meekes for stimulating discussions on phase diagrams and transitions.

References

[1] C. Ishimoto and T. Tanaka, Physical Review Letters **39**, 474 (1977).

[2] V. G. Taratuta, A. Holschbach, G. M. Thurston, D. Blankschtein, and G. B. Benedek, Journal of Physical Chemistry **94**, 2140 (1990).

[3] M. L. Broide, C. R. Berland, J. Pande, O. O. Ogun, and G. B. Benedek, Proceedings of the National Academy of Sciences of the United States of America **88**, 5660 (1991).

[4] Y. G. Kuznetsov, A. J. Malkin, and A. McPherson, Journal of Crystal Growth **232**, 30 (2001).

[5] M. Muschol and F. Rosenberger, Journal of Chemical Physics **107**, 1953 (1997).

[6] D. N. Petsev, X. Wu, O. Galkin, and P. G. Vekilov, Journal of Physical Chemistry B **107**, 3921 (2003).

[7] O. Galkin and P. G. Vekilov, Proceedings of the National Academy of Sciences of the United States of America **97**, 6277 (2000).

[8] P. G. Vekilov, Crystal Growth & Design **4**, 671 (2004).

[9] S. Tanaka, M. Ataka, and K. Ito, Physical Review E **65**, 051804 (2002).

[10] S. Tanaka, M. Yamamoto, K. Ito, R. Hayakawa, and M. Ataka, Physical Review E **56**, R67 (1997).

[11] S. Gorti, J. Konnert, E. L. Forsythe, and M. L. Pusey, Crystal Growth & Design **5**, 535 (2005).

[12] M. C. R. Heijna, M. J. Theelen, W. J. P. van Enckevort, and E. Vlieg, Journal of Physical Chemistry **111**, 1567 (2007).

[13] P. S. Chow, X. Y. Liu, J. Zhang, and R. B. H. Tan, Applied Physics Letters **81**, 1975 (2002).

[14] E. van Veenendaal, P. J. C. M. van Hoof, J. van Suchtelen, W. J. P. van Enckevort, and P. Bennema, Surface Science **417**, 121 (1998).

[15] S. Gorti, E. L. Forsythe, and M. L. Pusey, Crystal Growth & Design **4**, 691 (2004).

[16] J. Crank, *The mathematics of diffusion* (Oxford University Press, London, 1975), 2nd ed.

[17] MATLAB 6.5 (Release 13), The MathWorks Inc.

[18] M. Muschol and F. Rosenberger, Journal of Chemical Physics **103**, 10424 (1995).

[19] E. L. Forsythe, R. A. Judge, and M. L. Pusey, Journal of Chemical and Engineering Data **44**, 637 (1999).

[20] C. E. Kundrot, R. A. Judge, M. L. Pusey, E. H. Snell, Crystal Growth & Design **1**, 87-99 (2001).

[21] M. C. Robert, F. Lefaucheux, Journal of Crystal Growth **90**, 358-367 (1988).

[22] D. C. Carter, P. Rhodes, D. E. McRee, L. W. Tari, D. R. Dougan, G. Snell, E. Abolac, R. C. Stevens, Journal of Applied Crystallography **38**, 87-90 (2005).

[23] M. C. R. Heijna, P. W. G. Poodt, K. Tsukamoto, W. J. de Grip, P. C. M Christianen, J. C. Maan, J. L. A. Hendrix, W. J. P. van Enckevort, E. Vlieg, Applied Physics Letters **90**, 264105 (2007).